Medical Engineering & Physics 35 (2013) 549–554

Contents lists available at SciVerse ScienceDirect

Medical Engineering & Physics

journal homepage: www.elsevier.com/locate/medengphy

Technical note

Combining ultrasound-based elasticity estimation and FE models to predict 3D target displacement

Wissam Assaad, Sarthak Misra *

MIRA – Institute for Biomedical Technology and Technical Medicine, University of Twente, 7500AE Enschede, The Netherlands

ARTICLE INFO

Article history:
Received 20 April 2012
Received in revised form 16 October 2012
Accepted 4 November 2012

PACS:
87.10.Kn
87.19.R–
87.57.–s
87.85.G–
87.85.Ox
87.85.Pq
87.85.St

Keywords:
Computer-assisted surgical simulation
Finite element analysis
Minimally invasive surgery
Ultrasound

ABSTRACT

During minimally invasive surgical procedures (e.g., needle insertion during interventional radiological procedures), needle–tissue interactions and physiological processes cause tissue deformation. Target displacement is caused by soft-tissue deformation, which results in misplacement of the surgical tool (needle). This study presents a technique to predict target displacement in three-dimensions (3D) by combining soft-tissue elasticity estimation using an ultrasound-based acoustic radiation force impulse (ARFI) technique and finite element (FE) models. Three different phantoms with targets are manufactured, and subjected to varying loading and boundary conditions. Ultrasound images are acquired using a 3D probe during loading and unloading of each phantom, and subsequently target displacement is calculated. 3D FE models of the phantoms are developed, and they are used to predict target displacement. The maximum absolute error in target displacement between the experiments and FE analyses is found to be 1.39 mm. This error is less than the smallest tumor diameter (2.0–3.0 mm) which can be detected in breast tissue. This study shows that the combination of soft-tissue elasticity estimation using the ARFI technique and 3D FE models can accurately predict target displacement, and could be used to develop patient-specific plans for surgical interventions.

1. Introduction

Needle insertion is one of the most common minimally invasive surgical (MIS) procedure. It is generally performed in combination with various clinical imaging modalities, such as, computed tomography (CT) scans and X-ray, ultrasound and magnetic resonance (MR) images [1,2]. Tissue deformation and target (suspected lesion) displacement primarily occurs prior to needle puncturing the tissue [3]. Also, target displacement may result from patient motion or physiological processes [4]. Target displacement can result in misdiagnosis, and treatment may be delayed [5]. A patient-specific plan that predicts target displacement prior to the surgical procedure can lead to a more conclusive diagnosis [6,7].

Finite element (FE) analysis is one of the methods used to predict organ deformation and subsequently target displacement [8]. Developing the FE model requires the organ geometry, boundary conditions and constitutive model in order to predict organ deformation accurately. The organ geometry and its connectivity with the surrounding tissue can be determined by the previously mentioned imaging techniques, e.g., modeling the prostate and surrounding tissue using MR images [9]. Developing a constitutive model of the organ is difficult because soft-tissue is anisotropic, inhomogeneous and viscoelastic. The properties of soft-tissue vary significantly between *in vivo* and *ex vivo* measurements. Misra et al. [1] hypothesized that for MIS procedures, prior knowledge of the organ geometry, its surrounding boundary conditions and distribution of linear elastic properties can be used to accurately predict target displacements. They demonstrated this using two-dimensional (2D) FE analyses.

Previously Op den Buijs et al. [10] computed the relative elasticity of the target and its surrounding gel using ultrasound elastography and inverse FE analysis, and calculated target displacement using a 2D FE model. In this study, we extend and prove our hypothesis for the three-dimensional (3D) case. Further, target displacement is predicted by using a combination of an ultrasound-based acoustic radiation force impulse (ARFI) technique to estimate soft-tissue elasticity, and 3D FE analyses. The Young's modulus (absolute value) of the soft-tissue can be estimated directly by using the ultrasound-based ARFI technique [11], which is based on the shear wave velocity through tissue. This is in contrast to the ultrasound-based tissue compression strategies used to measure relative elasticity [12,13], which in some cases rely on the inverse

* Corresponding author. Tel.: +31 53 489 2704.
E-mail address: S.Misra@utwente.nl (S. Misra).

1350-4533/$ – see front matter © 2012 IPEM. Published by Elsevier Ltd. All rights reserved.
http://dx.doi.org/10.1016/j.medengphy.2012.11.003

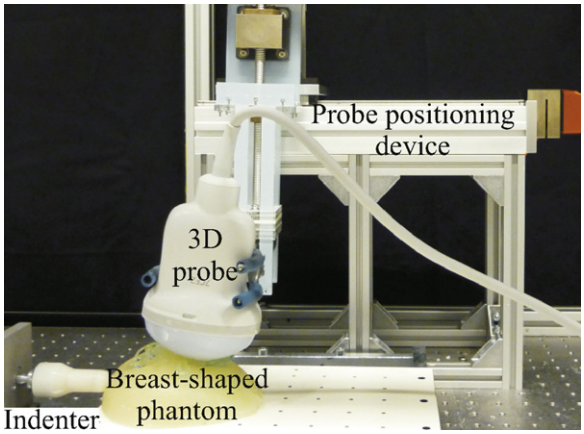

Fig. 1. Experimental setup: indentation causes displacement of the target which is embedded in the breast-shaped phantom. Target displacement is calculated by using a three-dimensional (3D) ultrasound probe.

FE analysis, and are subjected to convergence problems and hence, a time consuming procedure [10].

The novel aspect of this study is to confirm that soft-tissue elasticity estimation using an ultrasound-based ARFI technique can be incorporated in a geometrically accurate 3D FE model. This FE model is used to predict target displacement, which could be used in developing patient-specific plans for surgical interventions. In this study, different phantoms with targets are manufactured. The Young's moduli of the target and its surrounding gel are determined by using the ultrasound-based ARFI technique. FE analyses are performed in 3D with varying loading and boundary conditions. For each case, the displacement of the target is calculated and compared to the displacements computed from the images acquired by the 3D ultrasound probe (Fig. 1).

2. Experimental methods

The experimental setup consists of an indenter, ultrasound machine and a probe positioning device, as shown in Fig. 1. Experiments are performed on three different soft-tissue phantoms. The manufacturing process of the targets and the phantoms is detailed in Section 2.1. A target is embedded in each phantom to mimic a tumor within breast tissue. Section 2.2 presents the loading and boundary conditions that are used in the experiments and FE analyses. The calculation of the target displacement due to external loading using the acquired images is described in Section 2.3. The estimation of the Young's moduli of the target and its surrounding gel using an ultrasound-based ARFI technique is detailed in Section 2.4.

2.1. Manufacturing of soft-tissue phantoms

2.1.1. Target

Polyvinyl alcohol (PVA) (Sigma–Aldrich Chemie B.V., Zwijndrecht, The Netherlands) is used to manufacture the targets because they can be used in several experiments. The targets are manufactured by adding PVA to a container filled with water such that its percentage in the mixture is 10 wt%. The mixture is heated until the PVA is completely dissolved in water. The mixture is poured in a mold with spherical cavities in order to prepare the targets. The diameter of each cavity is 8 mm. The mold is kept at room temperature (∼21 °C). After 6 h at room temperature, the mold is stored in the freezer (∼−7 °C). After 14 h in the freezer, the mold is stored at room temperature for 10 h.

2.1.2. Phantoms

Gelatine (Dr. Oetker, Ede, The Netherlands), agar (Boom, Meppel, The Netherlands) and silica gel (particle size <63 μm SiC, E. Merck, Darmstadt, Germany) are added to a container filled with water. The mixture consists of 8 wt% gelatine, 1 wt% agar and 1 wt% silica. The silica gel is added to mimic the tissue acoustic scatter. The mixture is heated until the particles are completely dissolved in water. Three molds are prepared for manufacturing phantoms A, B and C. Phantoms A and B are shown in Fig. 2. Phantom C is shown in Fig. 3. The mold used to manufacture phantom C (breast-shaped phantom) is designed using SolidWorks 3D Computer Aided Design (CAD) software (Dassault Systemes SolidWorks Corp., Concord, USA) and printed by an Objet Eden250 3D printer (Objet Geometries Inc., Billerica, USA). The target is located at the center of each mold for phantoms A and B. The target is located at the mid-plane and 30 mm from the top of the mold for phantom C. The mixture is poured into the molds while the target is held within the mold by sewing pins. The sewing pins are fixed by wooden sticks. The wooden sticks are fixed to the mold walls. The molds are stored in the fridge (∼7 °C) for four days to reach stable elastic properties [10].

2.2. Loading and boundary conditions

Experiments and FE analyses are performed on phantoms A, B and C with varying loading and boundary conditions. The 3D probe is pushed 4 mm into phantom A for three different boundary condition cases as shown in Fig. 2 and described below.

- Case 1: the bottom and the four lateral sides are constrained in all directions (Fig. 2(a)).
- Case 2: similar to Case 1 but the constraint is removed from side 1 (Fig. 2(b)).
- Case 3: similar to Case 1 but the constraints are removed from sides 1 and 2 (Fig. 2(c)).

Phantom B is indented with a 16 mm diameter indenter. The indenter is pushed 6 mm along the negative x-axis into phantom B. During indentation the phantom is subjected to the following boundary condition:

- Case 4: the bottom and the side opposite to side 1 are constrained in all directions (Fig. 2(d)).

Phantom C is subjected to two different loading cases. For both cases, the phantom is fixed at the bottom side. The two cases are shown in Fig. 3 and described below.

- Case 5: the 3D probe is pushed 10 mm into phantom C (Fig. 3(a)).
- Case 6: phantom C is indented by a 16 mm indenter. The indenter is pushed 6 mm into phantom C (Fig. 3(b)).

FE models are developed for all the cases and these models are used to predict target displacement (Section 3.1).

2.3. Target displacement calculation

Target displacement is measured by the 3D probe 7CF2 which is compatible with ACUSON S2000 Ultrasound System (Siemens Medical Solutions, Erlangen, Germany). The probe is positioned on top of the phantom as shown in Fig. 1. Target displacement occurs by pushing the probe or pushing the indenter into the phantom. Ultrasound Digital Imaging and Communications in Medicine (DICOM) images are acquired both before and after target displacement. A MATLAB-based program (The Mathworks Inc., Natick, USA) reads each image, segments the target from the surrounding gel

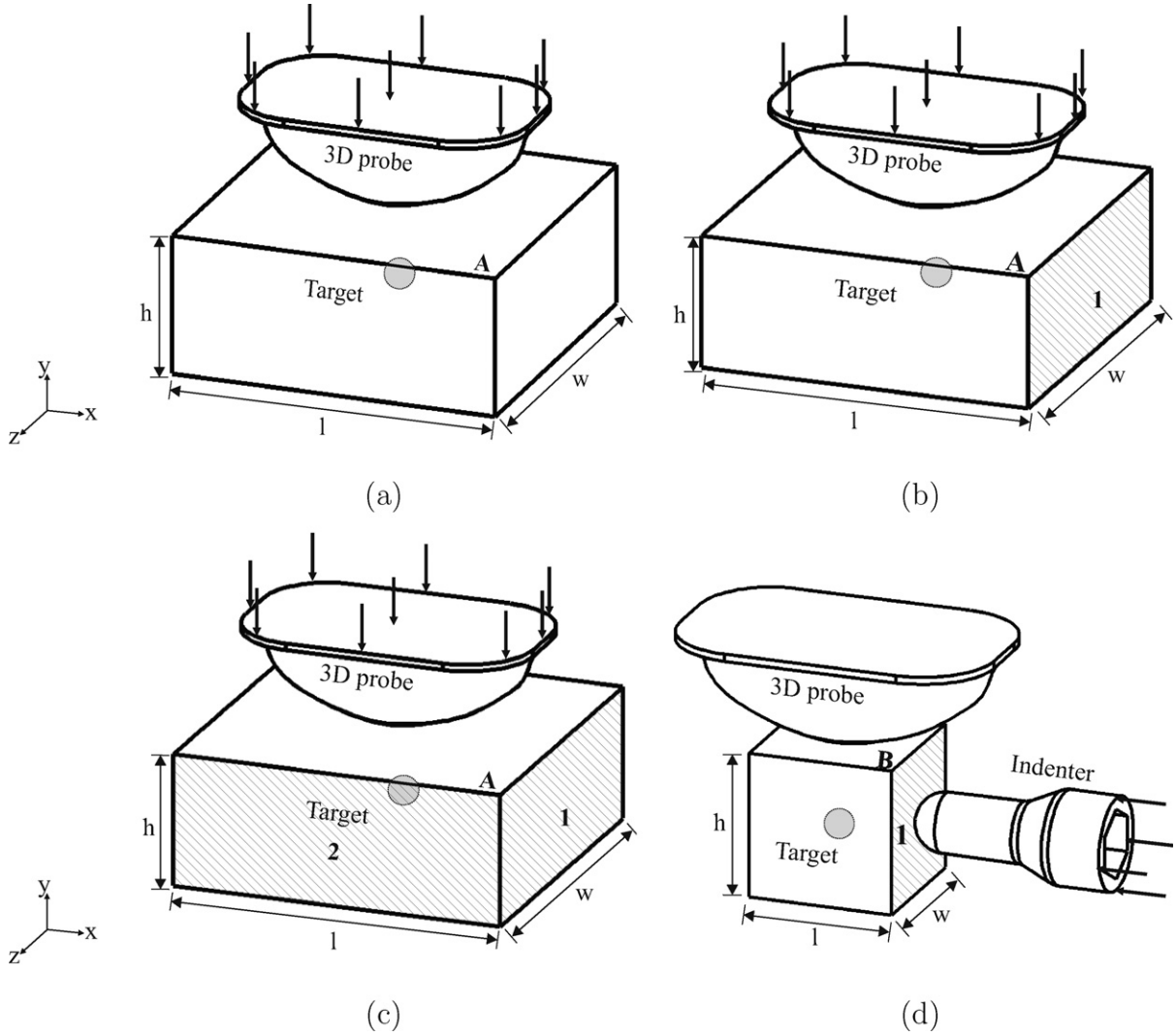

Fig. 2. Various loading and boundary condition cases applied to phantom A (l = 100 mm, w = 100 mm, h = 40 mm) and phantom B (l = 40 mm, w = 40 mm, h = 40 mm). The target diameter in each phantom is 8 mm. (a) Case 1, (b) Case 2, (c) Case 3 and (d) Case 4. Side 1 is unconstrained in Case 2. Sides 1 and 2 are unconstrained in Case 3.

and re-saves the images in DICOM format. The segmentation is performed by inverting the images to grayscale, increasing the contrast and inverting the images to binary such that the background color is black and the target color is white. These DICOM images are imported into the commercial program ScanIP (SIMPLEWARE LTD, Exeter, UK) to develop the 3D model of the target, and evaluate its center of gravity. The displacement of the target center of gravity due to external loading is calculated and is represented by the vector, **v** (Fig. 4).

2.4. Young's modulus estimation

The speed of the shear wave propagation in different regions of the phantom is measured by an ultrasound-based ARFI technique

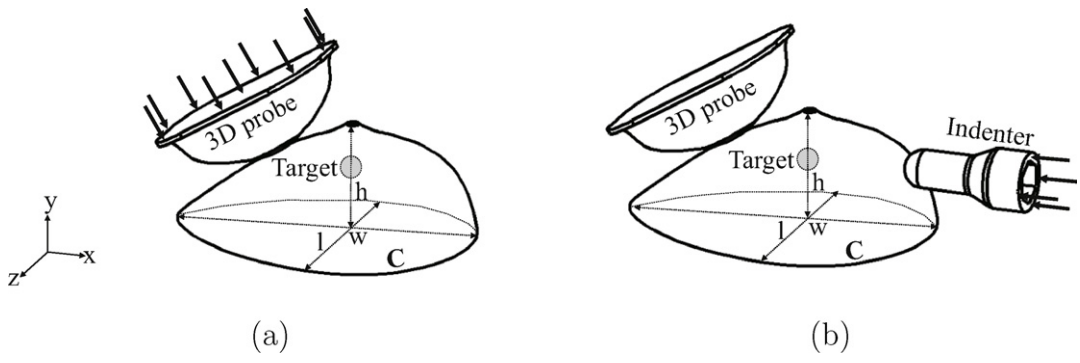

Fig. 3. Various loading and boundary condition cases applied to phantom C (l = 160 mm, w = 100 mm, h = 50 mm). The target diameter is 8 mm. (a) Case 5 and (b) Case 6. For the two cases, the phantom is fixed at the bottom side.

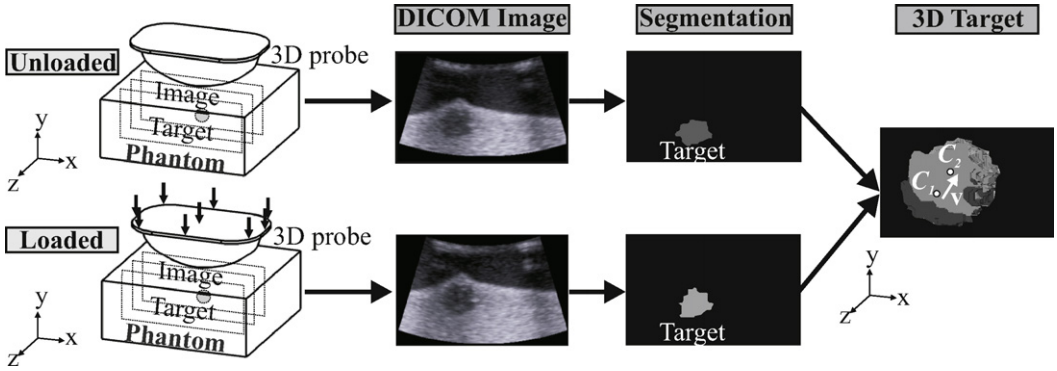

Fig. 4. Flow chart for target displacement calculation: the three-dimensional (3D) ultrasound probe is positioned on top of the phantom. The probe is pushed into the phantom. The position of the target changes under external loading. C_1 is the target center of gravity when the phantom is unloaded. C_2 is the target center of gravity when the phantom is loaded. The displacement vector of the target center of gravity is represented by **v**.

(Virtual Touch™ Tissue Quantification, Siemens AG Healthcare, Erlangen, Germany) [14]. It is observed that the speed is not constant in the phantom. The speed in the phantom is higher at the bottom half than at the top half due to the precipitation of the constituents in the mixture. In order to calculate the Young's modulus of the surrounding gel accurately, it is divided at its mid-plane into two regions, V_1 and V_2. The target is considered as one region, V_3, because the speed is observed constant in this region. The three regions are shown in Fig. 5. The material of the gel and the target are assumed isotropic, incompressible and linear elastic [11]. The Young's modulus in each region is calculated by

$$G = C^2\rho, \tag{1}$$

where G, C and ρ are the shear modulus, shear wave propagation speed and the density of each region, respectively. The density of regions, V_1, and V_2, are calculated by dividing measured mass of a sample cut from each region by the sample volume (10 mm × 10 mm × 10 mm).

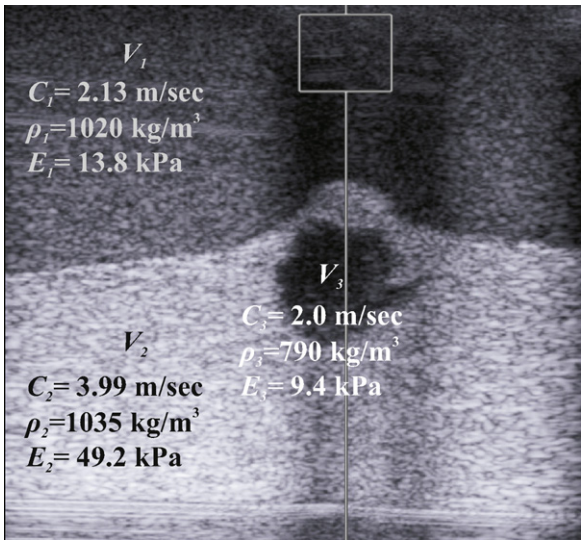

Fig. 5. An ultrasound-based acoustic radiation force impulse technique is used to calculate the elasticity (absolute value) of the phantom. The shear wave propagation speed (C), density (ρ) and Young's modulus (E) in regions, V_1, V_2 and V_3, in the phantom. The region, V_3, represents the target. In order to independently verify the estimated values, we measured the elasticity (36.7 ± 1 kPa) and density (1173 kg/m^3) of the phantom sample using a Dynamic Mechanical Analysis device (Physica MCR 501, Anton Paar, Graz, Austria) and pycnometer bottle, respectively.

The density of region, V_3, is calculated by dividing its measured mass by its volume. Using (1), the Young's Modulus is calculated by

$$E = 2(1+\nu)G, \tag{2}$$

where E and ν are the Young's modulus and the Poisson's ratio, respectively. The Poisson's ratio ν is equal to 0.495. The Young's moduli, E_1, E_2 and E_3, of the three regions are shown in Fig. 5 and are used as inputs in the FE model.

3. Results

This section presents the FE models used in predicting target displacement for phantoms A, B and C under varying loading and boundary conditions (Section 3.1). Further, the results of the FE analyses are compared with the data collected from the experiments, and described in Section 3.2.

3.1. Finite element model

The 3D models of the phantoms are imported into the commercial software ANSYS Mechanical (ANSYS Inc., Canonsburgh, USA). The models are discretized with 10-noded tetrahedron elements. For models of phantoms A, B and C, the Young's modulus is assigned to each region, and the corresponding loading and boundary conditions described in Section 2.2 are applied. The contact between the target and its surrounding gel is modeled as *bonded*. For Cases 1–3, a displacement of 4 mm is applied along the negative y-axis at the interface between the 3D probe and phantom A (Fig. 2(a)–(c)). For Case 4, a displacement of 6 mm is applied along the negative x-axis at the interface between the indenter and phantom B (Fig. 2(d)). For Case 5, the 3D probe is pushed by 10 mm into phantom C (Fig. 3(a)), while for Case 6, the indenter is pushed by 6 mm into phantom C (Fig. 3(b)). For all the cases, contact between the 3D probe and phantom, and the indenter and phantom is modeled as *frictionless*. Geometric non-linearity is considered in all the cases.

3.2. Target displacement prediction

For each case, the experiment is performed three times. The mean target displacement components in x-, y- and z-directions, and the mean of the resultants for each case are provided in Table 1. Also, the standard deviation of all the experimental values are tabulated. For each case, the absolute error in target displacement is calculated between the experiments and FE analyses. The maximum mean error is 1.39 mm, which is found in Case 5. This error is less than the smallest tumor diameter (2.0–3.0 mm) which can be detected in breast tissue [15].

Table 1
Target displacements along the x-axis, y-axis and z-axis from experiments (EXP) and finite element analyses (FEA). Mean of experimental target displacements are calculated as: $\bar{x} = ((\sum_{i=1}^{n} x_i)/n)$, $\bar{y} = ((\sum_{i=1}^{n} y_i)/n)$ and $\bar{z} = ((\sum_{i=1}^{n} z_i)/n)$, for $n = 3$ (three experimental trials for each case). The mean of the resultant of the experimental target displacements is $\bar{r}$ ($\bar{r} = ((\sum_{i=1}^{n} r_i)/n)$, where $r_i = \sqrt{x_i^2 + y_i^2 + z_i^2}$). The standard deviation values (within brackets) are reported for the experimental cases. The absolute error (e_*, for $^* = x, y, z$ and r) between EXP and FEA are also provided, where $e_r = \sqrt{e_x^2 + e_y^2 + e_z^2}$.

Case	Method	$\bar{x}$ (mm)	$\bar{y}$ (mm)	$\bar{z}$ (mm)	$\bar{r}$ (mm)
1	EXP	0.03 (0.04)	1.57 (0.06)	0.03 (0.04)	1.57 (0.06)
	FEA	0.02	1.80	0.00	1.80
	Error (e_*)	0.01	0.23	0.03	0.24
2	EXP	0.48 (0.04)	1.10 (0.10)	0.03 (0.06)	1.20 (0.10)
	FEA	0.67	1.80	0.00	1.92
	Error (e_*)	0.19	0.70	0.03	0.72
3	EXP	0.16 (0.06)	1.83 (0.11)	0.37 (0.18)	1.88 (0.10)
	FEA	0.54	1.83	0.48	1.96
	Error (e_*)	0.37	0.00	0.11	0.39
4	EXP	1.23 (0.00)	0.26 (0.11)	0.12 (0.10)	1.27 (0.03)
	FEA	1.34	0.48	0.10	1.42
	Error (e_*)	0.10	0.21	0.02	0.24
5	EXP	4.06 (0.15)	1.93 (0.11)	1.80 (0.13)	4.85 (0.12)
	FEA	4.10	0.80	1.00	4.29
	Error (e_*)	0.04	1.13	0.80	1.39
6	EXP	0.62 (0.47)	0.13 (0.06)	0.37 (0.10)	0.75 (0.43)
	FEA	0.46	0.13	0.14	0.50
	Error (e_*)	0.16	0.00	0.23	0.28

4. Discussion

In this study, we provide a method whereby elasticity properties of soft-tissue can be estimated *in vivo* using an ultrasound-based ARFI technique, and subsequently used in developing anatomically accurate patient-specific FE models to predict 3D target displacement during the pre-operative planning phase of a MIS procedure. The estimated elasticity value of the soft-tissue phantom in our study is within 15% of the independently measured value and hence, will not result in significant variation in target displacement prediction [10,16]. The relatively small errors in the target displacement could be due a combination of several modeling simplifications. These include the misalignment and contact conditions between the probe/indenter and phantom during the experiments and FE analyses. Further, friction between target and surrounding gel, and probe/indenter and phantom is not accounted for. The connections between target and surrounding gel, and probe/indenter and phantom are modeled as *bonded* and *frictionless*, respectively. In addition, targeting errors could be attributed to image processing, particularly while segmenting the target.

In this study we predict 3D target displacement under different loading and boundary condition cases using the combination of an ultrasound-based ARFI technique and 3D FE model. The tested boundary conditions are representative for biopsy cases, e.g., a breast preloaded holder device or (the lack of) anatomical support. The maximum absolute mean error is found to be 1.39 mm for the case where the 3D probe is pushed into the breast-shaped phantom (phantom C) by 10 mm (Case 5). This error is acceptable because it is less than the diameter of the smallest tumor (2.0–3.0 mm). Therefore, this study demonstrates the feasibility of predicting target displacement for developing patient-specific plans prior to a surgical procedure.

Funding

The Netherlands Organization for Scientific Research (NWO).

Acknowledgements

The authors would like to thank Gerben te Riet o/g Scholten and Alfred de Vries for preparing the phantom molds. This work is supported by funds from the Netherlands Organization for Scientific Research (NWO).

Conflict of interest

This is to certify that the authors have no financial or personal relationships with other people or organizations that would inappropriately influence our work.

References

[1] Misra S, Macura KJ, Ramesh KT, Okamura AM. The importance of organ geometry and boundary constraints for planning of medical interventions. Med Eng Phys 2009;31(2):195–206.
[2] Chen E, Mousavi P, Gill S, Fichtinger G, Abolmaesumi P. Ultrasound guided spine needle insertion. In: Proceedings of society of photo-optical instrumentation engineers (SPIE) conference, vol. 7625. 2010, 762538-1–8.
[3] Barbé L, Bayle B, de Mathelin M, Gangi A. Needle insertions modeling: identifiability and limitations. Biomed Signal Process Control 2007;2(3):191–8.
[4] Abolhassani N, Patel R, Moallem M. Needle insertion into soft tissue: a survey. Med Eng Phys 2007;29(4):413–31.
[5] Youk H, Kim E, Kim M, Lee Y, Oh K. Missed breast cancers at US-guided core needle biopsy: how to reduce them? Radiographics 2007;27:79–94.
[6] Dehghan E, Wen X, Zahiri-Azar R, Marchal M, Salcudean SE. Modeling of needle–tissue interaction using ultrasound-based motion estimation. In: Proceedings of medical image computing and computer-assisted intervention (MICCAI) conference, vol. 4971. 2007. p. 709–16.
[7] Fichtinger G, Fiene J, Kennedy CW, Kronreif G, Iordachita I, Song DY, et al. Robotic assistance for ultrasound-guided prostate brachytherapy. Med Image Anal 2008;12(12):535–45.
[8] Misra S, Ramesh KT, Okamura AM. Modeling of tool–tissue interactions for computer-based surgical simulation: a literature review. Presence 2008;17(5):463–91.
[9] Jahya A, Schouten MG, Fütterer JJ, Misra S. On the importance of modeling organ geometry and boundary conditions for predicting three dimensional prostate deformation. Comput Methods Biomech Biomed Eng, http://dx.doi.org/10.1080/10255842.2012.694876 in press.
[10] op den Buijs J, Hansen HHG, Lopata RGP, de Korte CL, Misra S. Predicting target displacements using ultrasound elastography and finite element modeling. IEEE Trans Biomed Eng 2011;58(11):3143–55.

[11] Palmeri ML, Wang MH, Dahl JJ, Frinkley KD, Nightingale KR. Quantifying hepatic shear modulus in vivo using acoustic radiation force. J Ultrasound Med Biol 2008;34(4):546–58.
[12] Ramalli A, Basset O, Cachard C, Tortolli P. Quasi-static elastography based on high frame-rate imaging and frequency domain displacement estimation. In: Proceedings of IEEE ultrasonics symposium (IUS). 2010. p. 9–12.
[13] Ramalli A, Boni E, Basset O, Cachard C, Tortoli P. High frame-rate imaging applied to quasi-static elastography. Acoust Imaging 2012;31(1): 11–8.
[14] D'Onofrio M, Galloti A, Mucelli RP. Tissue quantitative with acoustic radiation force impulse imaging: measurement repeatability and normal values in the healthy liver. Am J Roentgenol 2010;195(1):132–6.
[15] Kopans DB. Breast imaging. 3rd ed. Philadelphia: Lippincott Williams & Wilkins; 2006.
[16] op den Buijs J, Abayazid M, de Korte CL, Misra S. Target motion predictions for pre-operative planning during needle-based interventions. In: Proceedings of the international conference of the IEEE engineering in medicine and biology society (EMBC). 2011. p. 5380–5.